JOURNAL OF CATALYSIS 150, 388–399 (1994)

Selective Reduction of NO_x by Methane on Co–Ferrierites

II. Catalyst Characterization

Yuejin Li, Terry L. Slager, and John N. Armor[1]

Air Products and Chemicals, Inc., 7201 Hamilton Boulevard, Allentown, Pennsylvania 18195

Received April 4, 1944; revised August 16, 1994

Co–ferrierite, active for the selective NO reduction by CH_4, was characterized by X-ray photon spectroscopy and magnetic susceptibility measurements. The adsorption of NO and NO_2 was studied by diffuse-reflectance FTIR spectroscopy to discover which intermediates participate in the NO_x reduction. The valence state of cobalt in Co–ferrierite and other Co–zeolite catalysts was found to be 2+. The dominant NO species adsorbed on Co–Y, Co–ZSM-5, and Co–ferrierite is in a dinitrosyl form appearing at 1810 and 1897 cm^{-1} for Co–Y and 1810 and 1890 cm^{-1} for Co–ZSM-5 and Co–ferrierite. The mononitrosyl form of the adsorbed NO is a minor species appearing at 1930–1935 cm^{-1} on all three samples. The mononitrosyl species on all samples is extremely weakly adsorbed. The dinitrosyl species adsorbed on Co–ferrierite is strongly adsorbed and needs to be heated above 300°C to desorb. Interestingly, the weakly adsorbed mononitrosyl species is enhanced in an O_2 environment (100 Torr of O_2) and is now stable to 200°C. However, in an oxygen environment, the dinitrosyl species is less stable, desorbing at ~200°C. All adsorbed NO species disappear at >200°C in 100 Torr O_2, and adsorbed NO_2 species were observed. NO_2 adsorbed on Co–ferrierite shows a weakly adsorbed, covalent N_2O_5 in addition to stable species, such as nitro, nitrito, and nitrato species. Together with earlier kinetic and reaction studies, we suggest a mechanism for the selective reduction of NO_x by CH_4.

INTRODUCTION

For the past few years, there has been a growing interest in the use of light hydrocarbons, in place of ammonia, to selectively reduce NO_x in oxidizing environments (1–16). A common observation in these studies is that O_2 greatly enhances the NO_x conversion to N_2. Over cobalt-exchanged zeolites (Co–zeolites) this phenomenon was also observed. All hydrocarbons acted as reducing agents. In this oxidizing atmosphere, the hydrocarbons selectively react with NO_x species instead of being completely combusted. NO_2 formation on a catalyst surface is thought to be a necessary step for the NO reduction, and the presence of O_2 is needed to form this active NO_x species. This conclusion is supported by comparing the NO/hydrocarbon reaction with the NO_2/hydrocarbon reaction (2–4, 17); the former proceeds very slowly, while the rate of the latter is similar to that of the NO/O_2/hydrocarbon reaction. However, the transformation of NO to NO_2 on a catalyst under reaction conditions has not been observed. For the reduction of NO_x by hydrocarbons, CH_4 performs very differently from other hydrocarbons (18) and should be the most difficult to activate. In this regard, some Co–zeolites are remarkably active for the $NO/CH_4/O_2$ reaction. An understanding of how CH_4 is activated is a key to uncovering the mechanism for the $NO/CH_4/O_2$ reaction.

Although zeolites exchanged with various cations demonstrate considerable utility as catalysts for NO_x reactions, the choice of cation is crucial for selectively catalyzing NO reduction. For example, Cu–ZSM-5 is an effective catalyst for NO decomposition to N_2 and O_2 (19, 20) and for selective NO reduction with C_{2+} hydrocarbons (6–12). Co–ZSM-5, on the other hand, does not have appreciable activity for NO decomposition (13, 19) but is active for NO reduction with hydrocarbons (6, 21). Yet, Co–ZSM-5 is a good catalyst for the selective reduction of NO with CH_4, while Cu–ZSM-5 is not (13). The reaction and kinetic behaviors of these two catalysts must stem from the properties of cations in a zeolite environment. One way to probe the difference between these two systems is to study the adsorbed NO_x species with infrared spectroscopy (IR). While much work has been reported on the Cu–ZSM-5 system to understand the NO decomposition chemistry (22–27), similar work on Co–zeolites has not been reported except for earlier work on Co–Y (28–30). Co–ferrierite is the most active catalyst reported for the selective reduction of NO with CH_4 (15). This paper focuses on the characterization of Co–ferrierite catalyst with IR, X-ray photoelectron spectroscopy (XPS), and magnetic susceptibility measurements. It is meant to complement the companion paper (17) on NO_x (NO and NO_2)–catalyst interaction. These data allow us to specu-

[1] To whom all correspondence should be addressed.

0021-9517/94 $6.00

late on reaction mechanisms for the selective reduction of NO_x by CH_4 in O_2.

EXPERIMENTAL

Sample Preparation

The preparation of Co–zeolites was described previously (13–15). Both Co–ferrierite (Si/Al = 8 and Co/Al = 0.36) and Co–ZSM-5 (Si/Al = 11 and Co/Al = 0.49) samples were prepared by exchanging cobalt acetate with NH_4–ferrierite or NH_4–ZSM-5 at 70–80°C. Co–Y [Si/Al of 2.5, a Co/Al ratio of 0.67 (over exchanged) and some residual Na (Na/Al = 0.27)] was made by exchanging cobalt acetate into a Na–Y (LZ–Y52) at 80°C.

Diffuse-Reflectance Infrared Spectroscopy

Diffuse-reflectance infrared spectra were collected on a Nicolet 20SX FTIR spectrometer at a resolution of 0.5 cm^{-1} using a Harrick HVC-DRP environmentally controlled cell. A neat powder sample was packed in a sample holder and pretreated by heating to 450°C in vacuum *in situ* before adsorption of NO. High-temperature IR data were collected by increasing the cell temperature and holding at desired temperature while collecting 500 scans (18 min). The IR single-beam background spectrum of the pretreated zeolite, analyzed at 25°C, was subtracted from a single-beam spectrum to obtain the net IR intensities in Kubelka–Munk (MK) units. Since we are looking at qualitative changes in the spectra as a function of temperature, no adjustment was made to correct for the baseline shift due to the temperature difference between the higher temperature spectra and the background.

For all IR experiments, a catalyst was first pretreated *in situ* in the IR chamber by ramping the temperature at 1°C/min in vacuum or flowing N_2 to 450°C, holding for 1 h, and then cooling to room temperature. For room temperature static adsorption studies, a mixture of NO/He was admitted to the cell. Spectra were recorded in the presence of NO and after evacuation at room temperature. For temperature-dependent IR studies, a mixture of NO/He was flowed through the cell at room temperature then replaced by a He flow. The temperature was increased stepwise (50°C/step) to 350°C in flowing He (ramp rate = 2°C/min). At each temperature step, IR spectra were recorded. Detailed pretreatment information will be described in conjunction with experimental results.

X-ray Photoelectron Spectroscopy

XPS sputter depth profiling was used to determine the composition profile into the catalyst surface for several Co–ferrierite samples. The experiments were carried out on a Perkin–Elmer PHI 5000LS ESCA spectrometer equipped with both standard and monochromatic X-ray sources, a multichannel detector, and an Omni III lens system. High-resolution regional data were collected at 23.50 eV pass energy, 0.125 eV step, and 200 msec/step. The sputter profile data were conducted at 29.350 eV pass energy. Quantitative analyses were based upon standard PHI 5600 atomic sensitivity factors (without a transmission function correction routine). The takeoff angle was 45° and the analysis size was 800 μm^2. A 4-KeV Ar ion beam was used for sputtering. The raster pattern was 3 mm × 3 mm. A typical etch rate on NIST SiO_2/Si is 40 Å/min. The spectra were charge corrected to Si 2*P* = 102.2 eV.

Magnetic Susceptibility Measurements

Magnetic susceptibilities of Co–zeolite samples were measured with a magnetic susceptibility balance (MSB) (Johnson Matthey). All samples were thermally treated before measurement. A sample in fine powder form was packed into a sample tube (0.1–0.2 g, 1.5–4.0 cm long) and inserted into the cavity of the MSB to obtain a reading. *The mass magnetic susceptibility* (X_g) in cgs units was calculated based on the equation

$$X_g = CL(R - R_0)/(10^9 m), \quad [1]$$

where C = calibration constant of the balance ($C = 1.356$), L = sample length (cm), m = sample mass (g), R = reading for sample, and R_0 = reading for empty tube. The *molar magnetic susceptibility* (X_m) is obtained based on

$$X_m = X_g/[M], \quad [2]$$

where $[M]$ is the molar concentration of cobalt. The *effective magnetic moment* (μ_{eff}) in Bohr magneton (BM) is calculated based on

$$\mu_{eff} = 2.828\,(X_m T)^{1/2}, \quad [3]$$

where T is temperature in K.

RESULTS

Infrared Spectroscopy (NO Adsorption)

Figure 1 shows IR spectra of NO adsorbed on Co–Y with 9 Torr of NO (spectrum 1) and with subsequent evacuation for 1 h (spectrum 2). Upon exposure to 9 Torr NO, bands at 1800, 1813, 1898, and 1930 cm^{-1} were observed. The bands between 1800 and 1813 cm^{-1} and those between 1900 and 1930 cm^{-1} were not well resolved. After evacuation, only two bands at 1813 cm^{-1} and 1897 cm^{-1} (shifted from 1898 cm^{-1}) remained, and the band at 1813 cm^{-1} had some asymmetric character at low frequencies, suggesting that a small band at about 1800 cm^{-1} may

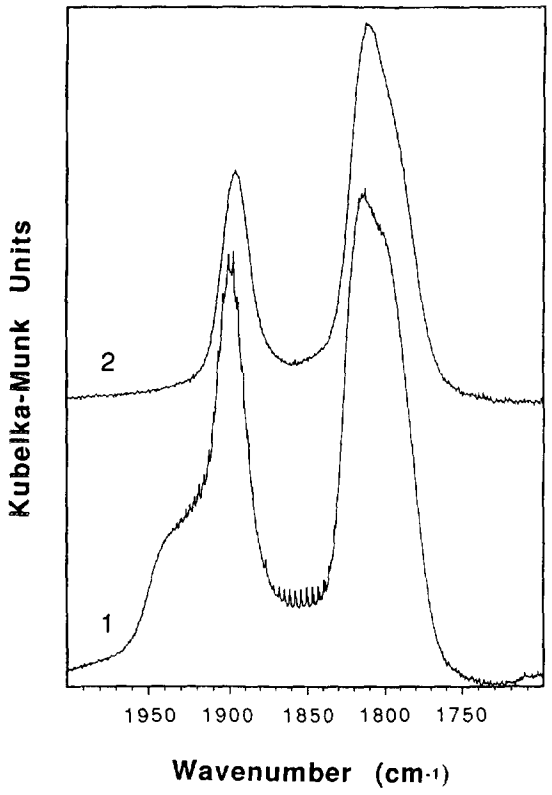

FIG. 1. Room temperature IR spectra of NO adsorbed on Co–Y in 9 Torr NO (1) and after evacuation (2).

be buried under the 1813 cm^{-1} band. The bands at 1813 and 1897 cm^{-1} are assigned to dinitrosyl species adsorbed on Co^{2+} with 1813 cm^{-1} being the asymmetric stretching frequency and 1897 cm^{-1} the symmetric stretching frequency. The dinitrosyl assignment is based on the work of Lunsford *et al.* (29) and Hall and co-workers (31) using labeled NO (mixture of ^{14}NO and ^{15}NO). At the beginning of NO adsorption (1 Torr), only one band at 1928 cm^{-1} was found, and the dinitrosyl bands were not observed. The dinitrosyl bands increased with time and pressure. At 9 Torr NO, the dinitrosyl bands appeared with high intensity and increased several fold in 3 h, whereas the intensity of the 1930 cm^{-1} band decreased with time. The angle (2θ) between the two adsorbed NO molecules on the same cation for the dinitrosyl species was calculated to be 119° based on (32)

$$I_{asym}/I_{sym} = \tan^2(\theta), \qquad [4]$$

where I is the integrated intensity of the IR band. This angle is in good agreement with values obtained by Hall and co-workers (116°) (31) and Lunsford *et al.* (123°) (29). Lunsford *et al.* (29) found the dinitrosyl bands at 1820 and 1905 cm^{-1} and two shoulders at 1800 and 1890 cm^{-1}. The species responsible for the shoulders was removed by evacuation at room temperature. The dinitrosyl bands were observed by Hall and co-workers (31) at 1901 and 1820 cm^{-1}. They observed three additional bands at 1928, 1886, and 1800 cm^{-1} whose intensities decreased with time.

A Co–ZSM-5 sample was exposed to 1 Torr of NO at room temperature for 30 min and then to 9 Torr of NO for 1 h. Figure 2 shows that the IR spectra collected after Co–ZSM-5 were exposed to 9 Torr of NO for 1 h (spectrum 1) and after evacuation for 1 h (spectrum 2). With both 1 and 9 Torr of NO, major bands at 1810, 1890, and 1935 cm^{-1} were observed. The bands at 1810 and 1890 cm^{-1} are due to cobalt dinitrosyl species, which are similar to those on Co–Y, and the band at 1935 cm^{-1} is tentatively assigned to a mononitrosyl species. Increasing NO partial pressure from 1 to 9 Torr increased the intensities of all bands. A higher degree of enhancement was observed for dinitrosyl bands. The intensity ratio of the dinitrosyl species (sum of two bands) to mononitrosyl species changed from 2.9 to 8.5 while increasing the pressure from 1 to 9 Torr NO. This suggests that the mononitrosyl species may be a precursor of the dinitrosyl species. The mononitrosyl band at 1935 cm^{-1} disappeared upon evacuation of the IR cell at room temperature (spectrum

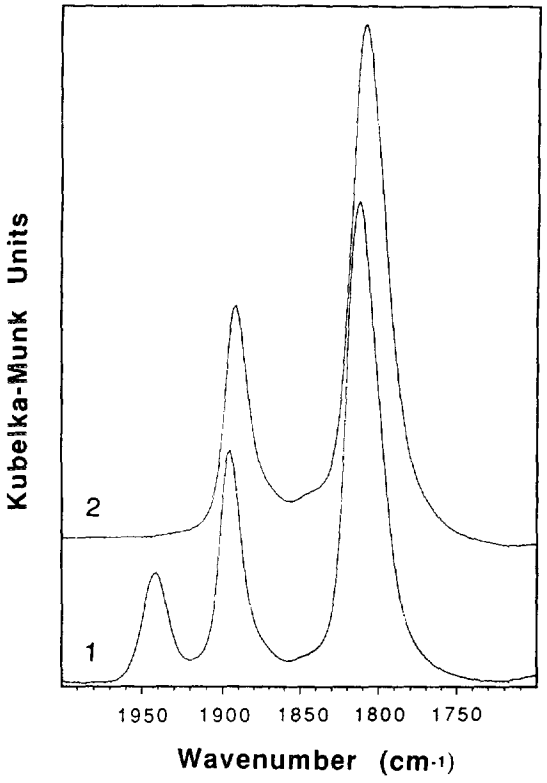

FIG. 2. Room temperature IR spectra of NO adsorbed on Co–ZSM-5 in 9 Torr NO (1) and after evacuation (2).

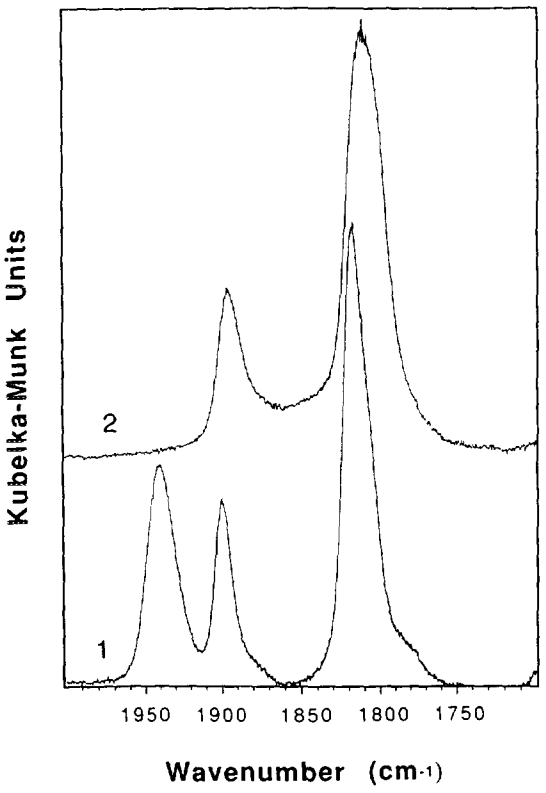

FIG. 3. Room temperature IR spectra of NO adsorbed on Co–ferrierite in 9 Torr NO (1) and after evacuation (2).

2). However, evacuation did not affect the intensities of the dinitrosyl bands. The dinitrosyl angle (2θ) was calculated to be 122°.

A variety of IR studies were performed on Co–ferrierite. Figure 3 compares the spectra obtained on the Co–ferrierite exposed to 9 Torr of NO at room temperature for 3 h (spectrum 1) and after subsequent evacuation at room temperature for 1 h (spectrum 2). As observed for Co–ZSM-5, with 9 Torr of NO, the two dinitrosyl stretching frequencies were found at 1815 and 1900 cm^{-1} and the mononitrosyl band was found at 1930 cm^{-1}. After evacuation, only the dinitrosyl bands remained (they shifted to 1807 and 1895 cm^{-1}, respectively), and their intensities were unchanged. When this sample was first exposed to 1 Torr of NO, the bands were very weak, especially the two dinitrosyl bands. Upon increasing the NO pressure to 9 Torr, the intensities of the two dinitrosyl bands increased dramatically (by a factor of 30) while that of the mononitrosyl band doubled. After a period of 3 h in 9 Torr of NO, the mononitrosyl band decreased substantially, whereas the dinitrosyl bands increased slightly. [The intensity ratio of the dinitrosyl bands to the mononitrosyl band is 2.5 in 9 Torr of NO.] The dinitrosyl species were very stable in vacuum; evacuation for an extended period of time did not change their intensities. The dinitrosyl angle was found to be between 127 and 133°.

The stability of adsorbed NO species on Co–ferrierite at elevated temperatures was studied under various conditions: (a) in vacuum, (b) with static 9 Torr of NO (He balance, total pressure = 900 Torr), and (c) in flowing He. Similar results were obtained under all three conditions. In Fig. 4, results obtained under flowing helium (condition c) are shown as a function of temperature. The Co–ferrierite sample was first pretreated *in situ*, by heating at 450°C under vacuum for 1 h. At room temperature, a NO/He mixture (1% NO) was passed through the IR chamber, and a spectrum was recorded (spectrum 1). A stream of He was then flowed through the chamber while increasing the temperature to 100°C. The temperature was subsequently increased to 150, 200, 250, 300, and 350°C in flowing He. A spectrum was collected 15 min after reaching each temperature. These spectra are labeled as 2, 3, 4, 5, 6, and 7 for 100, 150, 200, 250, 300, and 350°C, respectively.

At room temperature with a flowing 1% NO/He mixture, a small band at 1935 cm^{-1} was found due to mononitrosyl species but disappeared upon purging with He and

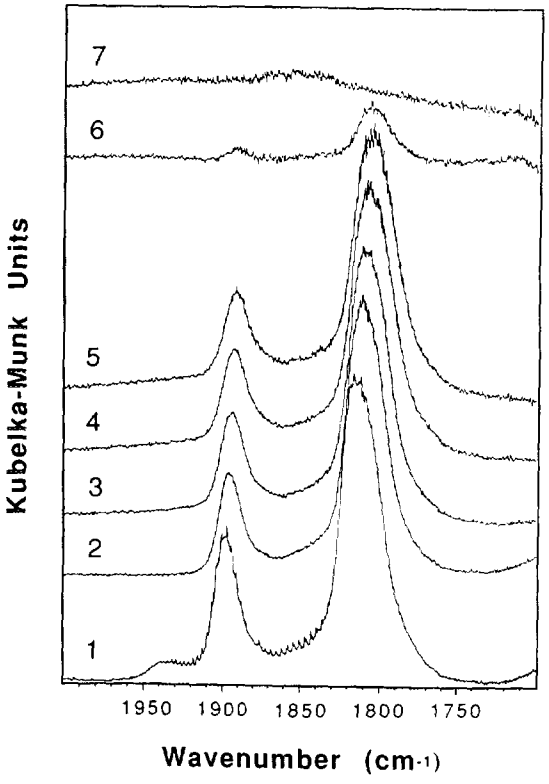

FIG. 4. IR spectra of NO adsorbed on Co–ferrierite as a function of temperature. Spectrum 1 was collected in flowing 1% NO/He mixture at 22°C; spectra 2, 3, 4, 5, 6, and 7 were collected in flowing He at 100, 150, 200, 250, 300, and 350°C, respectively.

TABLE 1

Temperature Dependence of IR Parameters of NO on Co-Ferrierite

Temperature (°C)	Adsorbed NO in flowing He			Adsorbed NO in 100 Torr O_2	
	$(NO)_2$ asym. (cm^{-1})	$(NO)_2$ sym. (cm^{-1})	Dinitrosyl angle, 2θ (°)	I_{1940}/I_{1815}	Dinitrosyl angle 2θ (°)
25	1816	1899	129	0.13	133
100	1815	1898	129	0.12	139
150	1812	1895	129	0.06	140
200	1810	1894	129	0.54	—
250	1808	1892	129	—	—

at elevated temperatures. The dinitrosyl species appear to be stable, and their intensities basically are unchanged up to 250°C. A substantial decrease in intensity was observed at 300°C, and no IR bands due to NO species were observed at 350°C.

Table 1 lists the band frequencies, intensity ratios, and dinitrosyl angles as a function of temperature. The frequencies of the dinitrosyl bands shifted downward with increasing temperature. This phenomenon was also observed in vacuum and with static (9 Torr) NO and appears to be the result of a weakened NO bond at elevated temperatures. The relatively high stability of NO species observed by IR spectroscopy is generally consistent with the temperature programmed desorption (TPD) experiments (17), where all NO molecules desorb below 300°C in flowing He. However, the TPD experiments show that NO molecules continued desorbing from the catalyst, while the IR experiment suggests little change in NO population below 250°C and a sharp decrease in IR intensity at temperatures beyond 250°C.

Infrared Spectroscopy (NO/O_2 Adsorption)

The effect of O_2 on adsorbed NO species was studied on this Co-ferrierite sample (Fig. 5). NO (9 Torr) was first adsorbed on this catalyst by flowing a 1% NO/He mixture at room temperature (spectrum 1). Oxygen (100 Torr O_2) was admitted into the chamber at room temperature after a 30-min evacuation (spectrum 2). The temperature was subsequently increased stepwise to 350°C in 100 Torr (static) O_2, with IR spectra recorded at each temperature. Interestingly, after admission of 100 Torr O_2 to the IR chamber, the mononitrosyl band at 1940 cm^{-1} was enhanced and its intensity changed little with increasing temperature to 200°C. The intensities of the dinitrosyl bands at 1813 and 1900 cm^{-1} were unchanged below 200°C but became undetectable above 250°C. The frequencies of dinitrosyl bands were constant with increasing temperature. Note that, in flowing He, 300°C is required to significantly reduce the dinitrosyl intensity (see Fig. 4). The intensity of the band at 1625 cm^{-1} became substantially higher at 200°C. Two other bands at 1600 and ~1560 cm^{-1} also appeared at $T > 250$°C. These new bands are assigned as adsorbed NO_2 species (*vide infra*) (24).

The mononitrosyl species on Co-ferrierite is unstable in vacuum or in flowing He even at room temperature. The presence of O_2 stabilizes the mononitrosyl species

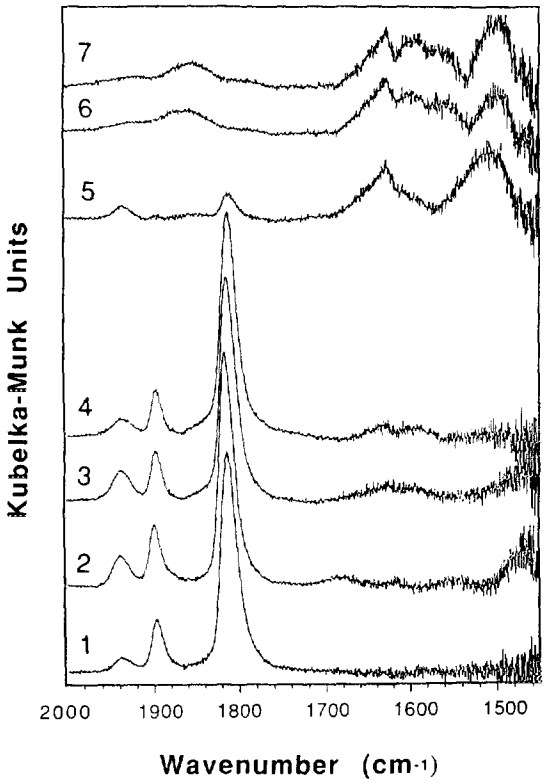

FIG. 5. IR spectra of NO adsorbed on Co-ferrierite—effect of O_2. Spectrum 1 was collected in flowing 1% NO/He mixture at 22°C; after a brief evacuation, spectra 2, 3, 4, 5, 6, and 7 were collected in 100 Torr O_2 at 22, 100, 150, 200, 250, and 300°C, respectively.

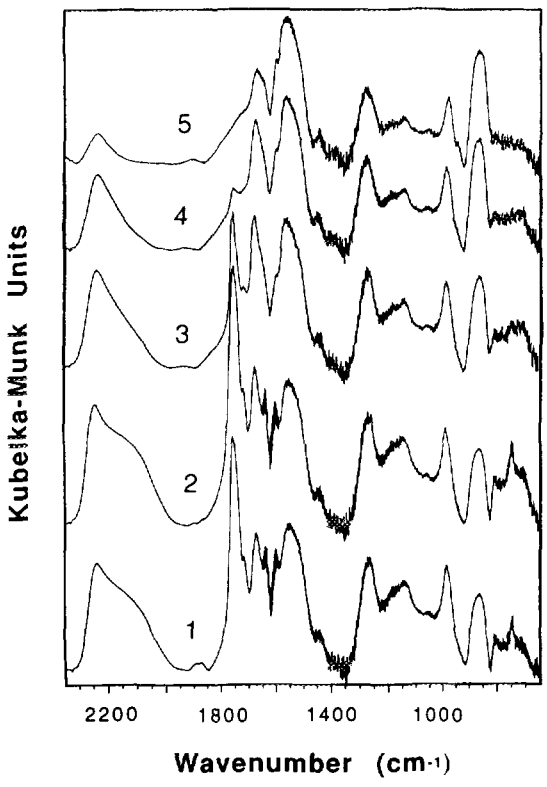

FIG. 6. Room temperature IR spectra of NO_2 adsorbed on Co-ferrierite. Spectra 1 and 2 were collected after flowing a 1% NO_2/He mixture through the IR cell at 25°C for 0.25 and 1.5 h, respectively. Spectra 3, 4, and 5 were collected after purging the cell with N_2 at 25°C for 1, 3.5, and 18 h, respectively.

on catalyst (see Fig. 5). Further, with O_2 the mononitrosyl species seems to be more stable than the dinitrosyl species at high temperatures; at 200°C the intensity ratio of the mononitrosyl band at 1940 cm^{-1} to the dinitrosyl band at 1815 cm^{-1} increased substantially compared to that at room temperature (by a factor of 4). At 200°C most of the dinitrosyl species was consumed to form NO_2 by reacting with oxygen, as shown by the simultaneous appearance of the adsorbed NO_2 species. The adsorbed NO_2 is the dominant NO_x species above 300°C. In the presence of oxygen the dinitrosyl angle (133–140°) also increased significantly compared to that in He (129°).

Infrared Spectroscopy (NO_2 Adsorption)

Figure 6 shows the IR spectra of adsorbed NO_2 on Co-ferrierite in a flowing 1% NO_2/He mixture and those after subsequent purge with N_2 at 25°C. Under flowing 1% NO_2/He at 25°C , sharp bands at 1751, 1705, and 740 cm^{-1} were immediately observed, which are assigned to adsorbed covalent N_2O_5 (33). These bands were weakened by flushing with N_2 at 25°C and eventually disappeared after the sample was flushed for 18 h at 25°C. In flowing NO_2/He, a pair of bands was also observed at 1635 and 1600 cm^{-1}. They have rotational fine structures, which are attributed to gaseous NO_2. These two bands immediately disappeared upon flushing the IR cell with N_2 at 25°C. A band with considerable intensity at 2230 cm^{-1}, along with a broad shoulder at 2100 cm^{-1}, was also observed with 1% NO_2/He flow. The intensities of these two bands decreased substantially with N_2 purge at 25°C, and the band at 2100 cm^{-1} disappeared after 18 h purge. These two broad bands may be attributed to weakly adsorbed NO_2 species. A strong band at 1540 cm^{-1} was observed upon adsorption of NO_2 and grew with N_2 purge. Two new bands at 1595 and 1627 cm^{-1}, which were not seen in NO_2/He flow, were detected with N_2 purge at 25°C. Several bands in the 1400–1000 cm^{-1} range (1270–1280, 1100–1140, 1040, 980 cm^{-1}) were detected upon exposure to NO_2 and appeared stable with extended N_2 purge. These bands (1400–1000 cm^{-1}) are tentatively assigned to adsorbed NO_3^- species (34).

Figure 7 shows temperature-dependent IR spectra of adsorbed NO_2. The broad band at ~2230 cm^{-1} disappeared upon heating to 100°C in N_2. The bands at 1627, 1595, and 1540 cm^{-1} are well resolved at elevated tempera-

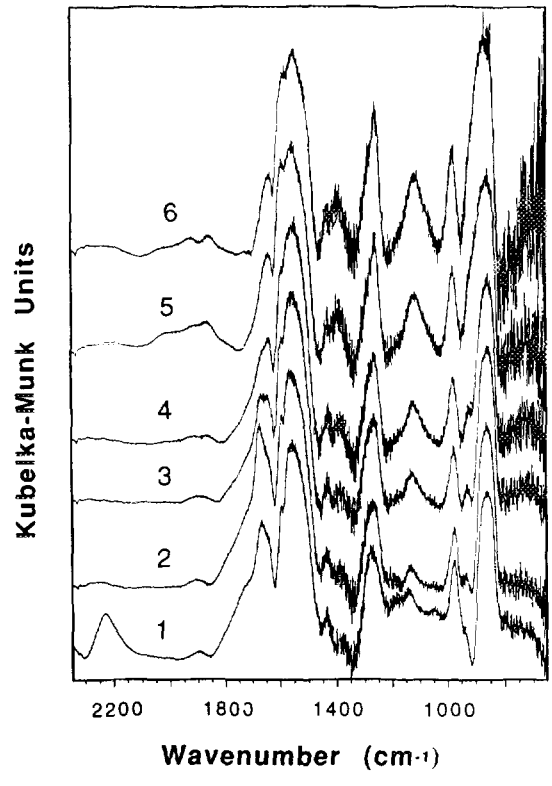

FIG. 7. IR spectra of NO_2 adsorbed on Co-ferrierite, as a function of temperature. After N_2 purge at room temperature for 18 h (see Fig. 6), spectra 1, 2, 3, 4, 5, and 6 were recorded in flowing N_2 at 25, 100, 150, 200, 250, and 300°C, respectively.

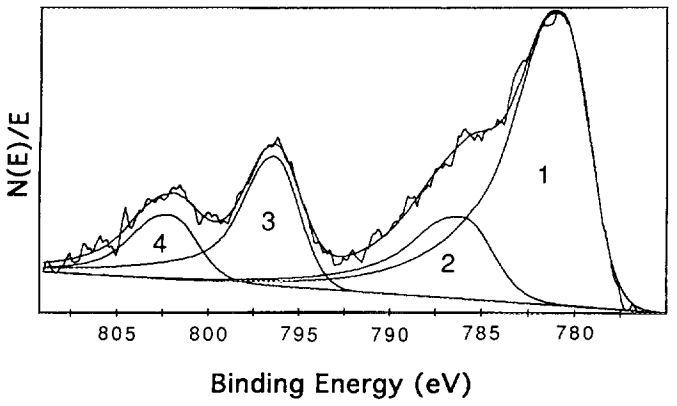

FIG. 8. XPS spectrum (Co 2*p* lines) of Co–ferrierite (Si/Al = 8, Co/Al = 0.39). This sample was pretreated with a CH_4/He mixture at 500°C for 2 h and subsequently purged with He for 1 h at the same temperature.

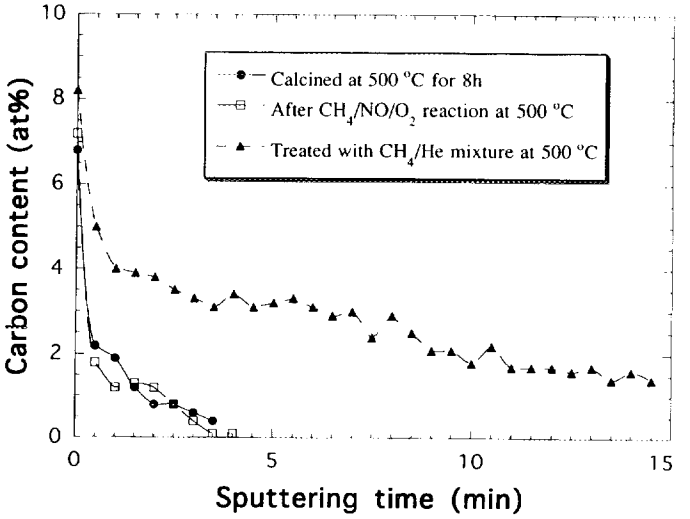

FIG. 9. XPS in-depth analysis of carbon intensity on a Co–ferrierite catalyst (Si/Al = 8, Co/Al = 0.39) pretreated at various conditions as a function of Ar sputtering time.

tures (>25°C), and they decreased slightly with increasing temperature. These three bands are assigned to adsorbed nitro, nitrito and nitrato species, respectively (31). The intensities of the low-frequency bands (1400–1000 cm^{-1}) were enhanced with increasing temperature and are stable at 300°C.

X-Ray Photoelectron Spectroscopy (XPS)

Figure 8 shows an XPS spectrum of Co 2*p* lines for Co–ferrierite (Si/Al = 8, Co/Al = 0.39) and its deconvolution; Table 2 summarizes the curve fittings. This sample was calcined at 500°C in air for 8 h and then treated with a CH_4/He mixture for 2 h at 500°C. [This part of the study was aimed at determining if there was carbon deposition.] Curve fitting analyses were carried out on the high-resolution data before sputtering with Ar^+. The binding energy for cobalt was found at 780.7 eV for $2p_{3/2}$ line and 796.4 eV for Co $2p_{1/2}$ line with two shake-up peaks at 786.0 and 802.1 eV, respectively. (The binding energies were charge corrected to Si2*p* = 102.2 eV). To check for the possibility of carbon deposition during NO_x reduction, we conducted XPS analyses on a Co–ferrierite catalyst which underwent three different thermal treatments: (a) calcination in air at 500°C for 8 h; (b) steady-state $CH_4/NO/O_2$ reaction at 500°C for 2 h followed by cooling in He to room temperature; and (c) a CH_4/He mixture (1000 ppm) flowing through the catalyst at 500°C for 2 h then cooled to room temperature in He. [These samples were exposed to air before XPS analysis.] A carbon depth profile of these three samples was obtained with Ar^+ sputtering (Fig. 9). For pretreatments (a) or (b), the carbon level of the sample quickly dropped to zero with Ar^+ sputtering (4 min), suggesting that during a steady-state $CH_4/NO/O_2$ reaction no detectable carbon accumulated. The initial carbon intensity is due to adventitious carbon. Clearly, the CH_4/He treated sample (pretreatment c) deposited carbon. The XPS C(1*s*) spectrum (not shown) is asymmetric and has a binding energy of 283.9 eV, suggesting a graphitic carbon species. In addition, there is no detectable change in binding energy for the Co 2*p* lines for all three pretreatments, and their line shapes are the same.

TABLE 2

Curve Fitting Summary for Co–Ferrierite

Band no.	BE (eV)	Band separ. (eV)	FWHM (eV)	% of total area
4	802.1	21.4	3.4	9.9
3	796.4	15.7	3.2	19.4
2	786.0	5.3	3.8	17.0
1	780.7	0.0	3.4	53.6

Magnetic Susceptibility Measurements

Table 3 summarizes the measurements of several cobalt-containing samples. The magnetic moment of an element is produced by the unpaired electrons of that element. As shown in Table 3, all the magnetic moments are in the range of 4.6–6 BM.

DISCUSSION

High spin Co^{2+} has 3 unpaired electrons and thus is paramagnetic. Typically, Co^{3+} does not have unpaired electrons and is diamagnetic. [The magnetic moment for Co^{3+} should be zero.] Based on this, we conclude that the cobalt in these calcined samples is divalent. The calcu-

TABLE 3

Magnetic Susceptibility Measurements of Cobalt-Containing Samples[a]

Sample	[Co] (mmol/g)	Sample mass (g)	L (cm)	R_0[b]	R[b]	X_g[c] $\times 10^6$	μ_{eff} (BM)
Co–ZSM-5[d]	0.68	0.149	3.60	−22	198	7.2	5.0
Co–ZSM-5[e]	0.68	0.134	3.45	−28	313	10.0	6.0
Co–Y[f]	2.00	0.136	3.55	−28	505	18.9	4.6
Co–ferrierite[g]	0.62	0.105	3.70	−28	116	6.9	5.0
Co/silica–alumina[h]	0.51	0.163	3.60	−28	181	6.3	5.4

[a] All samples were calcined at 500°C for 2 h before the magnetic measurements, except as indicated.

[b] R_0 is balance reading of the empty sample cell and R is the reading of sample + cell.

[c] X_g is in cgs units.

[d] Co–ZSM-5 has a composition of Si/Al = 11, Co/Al = 0.49, Na < 0.02 wt%.

[e] This sample was used as prepared (without high-temperature calcination).

[f] Co–Y has a composition of Si/Al = 2.5, Co/Al = 0.67, Na/Al = 0.27.

[g] Co–ferrierite: Si/Al = 8.5 and Co/Al = 0.39 with H^+ as a remaining cation.

[h] Co/silica–alumina was made by exchanging Co^{2+} into amorphous silica–alumina (Si/Al = 14), with 2.98 wt% Co.

lated spin-only magnetic moment of Co^{2+} for three unpaired electrons is 3.87 BM. In octahedral Co^{2+} complexes, the ground state is $^4T_{1g}$ and a large orbital contribution to the moment is expected. A magnetic moment value of 4.3 to 5.2 BM is usually observed (35). The ground state for tetrahedral Co^{2+} complexes is $^4A_2$ and a low moment approaching the spin-only value might be expected. However, an excited magnetic state in the tetrahedral complexes can be mixed with the ground state. Moments in the range from 4 to 5 BM have been predicted and were found experimentally (35).

Although the magnetic measurements unambiguously identify the cobalt ions as high spin, divalent ions, it is very difficult to determine the coordination of the cobalt ions based only on the magnetic moments because different coordination geometries have moment ranges which overlap. It is well known that hydrated cations in zeolite are octahedrally coordinated with 6 H_2O molecules; we observed a moment of 6.0 BM for hydrated Co–ZSM-5. Upon calcination at 500°C, the moment dropped to 5.0 BM, which is identical to that of a calcined Co–ferrierite catalyst. Co/silica-alumina has a moment of 5.4 BM, and an octahedral coordination is expected in this case. Co–Y has a relatively low moment, 4.6 BM. At first it seems that Co in zeolite Y has more of a tetrahedral character, but by careful analysis of the composition, one can conclude that this is due to the excess cobalt in the Y zeolite. This zeolite has 27% Na remaining in zeolite, yet a calculation based on the observed Co content shows that it contains 134% of the Co needed to fully replace all of the cations: about half of the Co may be precipitated. It is known that calcination of cobalt salt at 400–500°C results in Co_3O_4 which is a mixed valence (II, III) cobalt oxide, where Co^{2+} ions (1/3 of total cobalt ions) are in the tetrahedral interstices and Co^{3+} ions are in the octahedral interstices. We determined experimentally that pure Co_3O_4 has a moment of only 2.5 BM. Therefore, it is conceivable that the excess cobalt (not at the exchangeable sites) formed Co_3O_4 species during calcination which lowered the average magnetic moment for this Co-Y.

The difference in Co 2p binding energy between Co^{2+} and Co^0 is easily identifiable (2 eV), but the binding energies of Co^{2+} and Co^{3+} are indistinguishable. Thus, the appearance of shake-up satellite peaks can be used as an indicator to identify the valance state of cobalt. Shake-up satellites arise from the excitation of cobalt core electrons to a unfilled valence level. High spin Co(II) compounds normally have intense satellite bands associated to their 2p lines, while satellite bands for the low spin Co(III) compounds are either weak or missing (36). The strong satellite bands observed in this Co 2p spectrum suggest that the cobalt in ferrierite is Co^{2+} in paramagnetic, high spin state.

From the IR studies, it is clear that a dinitrosyl complex is formed upon exposure of NO to Co^{2+}-exchanged Y, ZSM-5, and ferrierite, and this dinitrosyl complex is the dominant NO species and is relatively stable. The frequencies of the dinitrosyl species on these three samples are remarkably similar (1810 and 1897 cm^{-1} on Co–Y, 1810 and 1890 cm^{-1} on Co–ZSM-5 and Co–ferrierite). Based on the NO adsorption studies, the electronic properties of Co^{2+} are similar for all three samples; the frequencies of dinitrosyl bands are close to the free NO frequency (1875 cm^{-1}). Perhaps little electron transfer between the NO species and Co^{2+} occurs (28). However, the notable increase in the dinitrosyl angle indicates that the coordination geometries for these samples are not the same. We suspect that this is caused by the differences within the channel structures. IR spectroscopy alone cannot explain why Co–Y is less active for the $NO/CH_4/O_2$ reaction.

Interesting comparisons can be made between cobalt-exchanged zeolite and Al_2O_3-supported cobalt oxide. More than a decade ago, Tøpsøe and Tøpsøe reported infrared spectra of NO adsorbed on a series of calcined Co/Al_2O_3 samples in comparison with those on Co_3O_4, $CoAl_2O_4$, and $Mo/Co/Al_2O_3$, an HDS catalyst (37). Only dinitrosyl bands were reported on Co/Al_2O_3 with the asymmetric stretching frequency at 1780–1795 cm^{-1} and the symmetric stretching frequency at 1860–1870 cm^{-1}. The frequencies shifted down with increasing Co loading, which they attributed to the contribution of the Co_3O_4 phase to the higher Co loaded Co/Al_2O_3 samples. The dinitrosyl angles obtained on these Co/Al_2O_3 samples are

TABLE 4

Infrared Parameters for NO Adsorbed on Cobalt-Containing Samples

Sample	Dinitrosyls: Asymetric (cm^{-1})	Symtric (cm^{-1})	Angle 2θ (°)	Mononitrosyls (cm^{-1})	Ref.
Co–Y	1810[a]	1897[a]	119	1930[b],1800[b]	This work
	1820[a]	1901[a]	116	1928[b],1886[b],1800[b]	30
	1820[a]	1905[a]	123	1890[b],1800[b]	28
Co–ZSM-5	1810[a]	1890[a]	122	1935[b]	This work
Co–ferrierite	1810[a]	1890[a]	130	1930[b]	This work
Cu–ZSM-5	1730[b]	1824[b]	104	1900[a,c],1810[d]	22–24
	1734	1827	104	1911[a,c],1811[d]	26
	1734	1827	102	1895[c], 1812[d]	25

Note. (*a*) Dominant; (*b*) unstable at RT; (*c*) NO^+–Cu^{2+}, stable; (*d*) NO^-–Cu^+.

between 120 and 130°, which are quite similar to those for Co–zeolites. They showed evidence suggesting the surface Co atoms that are capable of adsorbing NO are in octahedral coordination, probably occupying the octahedral vacancies in Al_2O_3 lattice. On the other hand, the NO intensity on Co/Al_2O_3 decreased dramatically with increasing evacuation temperature (a decrease of a factor of 8 with increasing temperature from room temperature to 117°C). The amount of irreversibly adsorbed NO on Co/Al_2O_3 at room temperature was also much smaller than we observed for Co–zeolites. The amount of NO adsorbed on Co/Al_2O_3 is a function of Co loading. The maximum amount of NO adsorbed per Co was reported as 1.05 mol/mol Co using a 0.26% CO/Al_2O_3 sample, which is much smaller than the ratio on Co–ZSM-5 or Co–ferrierite. [The ratio is 1.6 and 1.5 for Co–ZSM-5(14)-98 and Co–FER(8)-74, respectively (14, 17).] Based on the above comparisons, one can picture different environments Co^{2+} in a zeolite and on an Al_2O_3 surface despite the apparent similarity in dinitrosyl angle.

The difference among transition metal ions in catalyzing NO reactions is exemplified by Cu–ZSM-5 and Co–ZSM-5. The former is an active catalyst for the direct decomposition of NO to its elements (19, 20) but a poor catalyst for NO/CH_4 reaction in excess O_2 due to its low CH_4 selectivity (13). However, Co–ZSM-5 is inactive for NO decomposition but is an effective catalyst for the NO/CH_4 reaction promoted by gaseous O_2. It is interesting to examine the distinct ways in which these metal cations interact with NO species. [IR data for Cu–ZSM-5 and Co–zeolites are summarized in Table 4.] For Cu–ZSM-5, the dinitrosyl bands at 1734 and 1827 cm^{-1}, reportedly adsorbed on the Cu^+ sites, are unstable and are converted to a mononitrosyl band at ~1900 cm^{-1} with time or temperature due to oxidation of Cu^+ to Cu^{2+} by the adsorbed NO (22–27). The band at 1900 cm^{-1} assigned as $NO^{\delta+}$ on Cu^{2+} is the dominant band under most conditions. The valence state of a copper ion is readily changeable with increasing temperature ($Cu^{2+} \rightarrow Cu^+$) or upon interaction with NO at room temperature ($Cu^+ \rightarrow Cu^{2+}$). The ability of Cu^{2+} to accept an electron stabilizes the mononitrosyl band at ~1900 cm^{-1}. The stabilization of this NO species is the result of the transfer of an antibonding electron from a NO molecule to Cu^{2+}. This electron transfer increases the NO frequency (relative to the gas phase NO, ~1875 cm^{-1}) to 1900 cm^{-1}. Because of the high reactivity of Cu ions with NO molecules, disproportionation (N_2O and NO_2) and oxidation (NO_2) products were often observed during IR measurements. The redox property of Cu–ZSM-5 is thought to be an essential factor for NO decomposition. The facile redox process on copper sites in Cu–ZSM-5 is probably one reason for the instability of the dinitrosyl species.

Cobalt ions in Co-ZSM-5, however, have a valence state of 2+. They are not easily reducible to Co^+ or Co^0 and are very difficult to oxidize to Co^{3+} (14). This is supported by XPS results; even after high-temperature treatment with CH_4 the valence state of cobalt is still 2+. A stable NO^- species is not observed due to the poor electron-donating property of the Co^{2+} ion in ZSM-5. However, a minor, weak $NO^{\delta+}$ species can be formed (the band at 1935 cm^{-1}), which disappears upon evacuation. A salient difference between $Co^{2+}$and Cu^{2+} in NO adsorption is the stability of dinitrosyl species. The dinitrosyl species on Co^{2+} is stable even at high temperatures, e.g., 300°C. In addition, the stability of the dinitrosyls may be related to the angles between the nitrosyls. The relatively small angle on Cu–ZSM-5 (104°) means a shorter distance for the two N atoms, increasing the interaction between the two nitrosyl groups. This may induce a reaction to produce N_2O and O(a) or desorption of one NO to form a mononitrosyl species. Conversely, the wide angles between the two nitrosyls on Co–ZSM-5 (122°) and other Co–zeolites provide an environment which stabilizes the dinitrosyls, which may be a reason why Co–zeolites are not active for the direct NO decomposition. On the other hand, the adsorbed NO_x species are stable enough at high temperatures to carry out catalytic reaction with hydrocarbons, e.g., CH_4.

The dominant form of NO adsorbed on Co–ferrierite is the dinitrosyl species, which is so stable that 350°C is needed to desorb it. On the other hand, the mononitrosyl band at 1930 cm^{-1} is a minor species that can be easily removed by evacuation at room temperature or by flushing with He. Interestingly, this mononitrosyl species can be stabilized by O_2, allowing the mononitrosyl species to

remain on Co^{2+} sites up to 200°C. This suggests that Co^{2+} cations in ferrierite are coordinately unsaturated and can accommodate two more ligands upon exposure to gaseous NO. It seems that a mononitrosyl species can be stabilized only by coadsorption of another oxygen atom on the same Co^{2+}, which further transforms to an adsorbed NO_2 species at higher temperatures (≥250°C). The disappearance of dinitrosyl species at 250°C in the presence of O_2 (instead of 350°C in He) and simultaneous growth of the band at 1625 cm^{-1} suggest the transformation of a dinitrosyl species to the adsorbed NO_2 species by reaction with O_2 at elevated temperatures. IR data illustrate that the dinitrosyl bands (1810 and 1900 cm^{-1}) are mainly replaced by the NO_2 bands at 1630 and 1600 cm^{-1} at 200°C, and the mononitrosyl band at 1930 cm^{-1} is replaced by the band at 1560 cm^{-1}. This process can be illustrated by the following scheme:

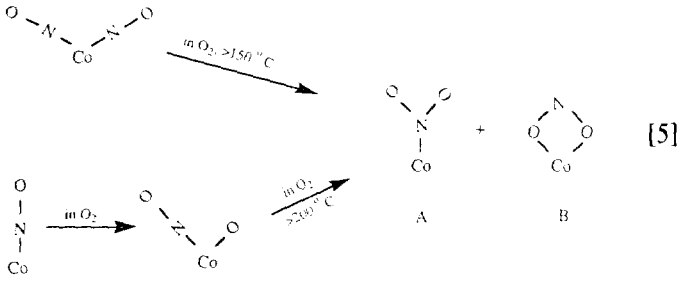

[5]

This is consistent with the TPD results. In flowing O_2 the NO desorption feature at $T > 200$°C was absent compared to results in flowing He. Perhaps it is transformed to an adsorbed NO_2 species ([5A] or [5B] above). [NO_2 could not be accurately measured with our residual gas analyzer (RGA) because of severe fracturing by the electron beam.]

The state of NO_x species adsorbed on Co–ferrierite at low temperatures may not be involved directly in the NO reduction which occurs at high temperatures. However, their transformation from mono- or dinitrosyl species in O_2 during increasing temperature is important in identifying the active species on the catalyst. This process also explans the role of O_2 in the NO catalysis and supports the observations (17) made for the $NO/CH_4/O_2$ or NO_2/CH_4 reaction. That is, the role of O_2 is to convert NO to adsorbed NO_2 species. It appears that the strongly adsorbed NO_2 species is most relevent to the high-temperature catalysis. The interconversion of NO and NO_2 species in the gas phase or on the catalyst is a reversible reaction controlled by thermodynamic equilibrium. An increase in NO pressure linearly increases the concentration of catalyst-bound NO_2 species, and as a consequence increases the overall rate of reaction, which was observed experimentally (13, 15).

Another objective of our IR work was to identify intermediate species present during the NO_x reduction. An *in situ* IR measurement was attempted during a steady-state NO_2/CH_4 reaction at 400°C, but no measurable IR signal of adsorbed species was detected. This may be due to extremely small amounts of adsorbed molecules on the catalyst at this temperature. Direct evidence for C–N bond formation during the NO_x/CH_4 reaction remains as a challenge and provides a basis for future research.

To address possible pathways for the NO reduction reaction, two important questions need to be asked: (a) how is CH_4 activated and (b) how is a N–N bond formed? Drawing upon the results of our previous publications (13–15, 17, 21) and an earlier presentation (38), we can suggest a possible stepwise mechanism:

$$Z\text{–}Co + NO \rightleftarrows Z\text{–}Co\text{–}NO \quad [6]$$

$$Z\text{–}Co\text{–}NO + 1/2O_2 \rightleftarrows Z\text{–}Co\text{–}NO_2 \quad [7]$$

$$CH_4 + Z\text{–}Co\text{–}NO_2 \rightarrow CH_3\cdot + Z\text{–}Co\text{–}HNO_2 \quad [8]$$

$$CH_3\cdot + Z\text{–}Co\text{–}NO_2 \rightarrow Z\text{–}Co\text{–}NO_2CH_3 \quad [9]$$

$$Z\text{–}Co\text{–}NO_2CH_3 + NO \rightarrow N_2 + CO + H_2O + Z\text{–}Co\text{–}OH \quad [10]$$

$$Z\text{–}Co\text{–}OH + NO \rightarrow Z\text{–}Co\text{–}HNO_2 \quad [11]$$

$$2Z\text{–}Co\text{–}HNO_2 \rightarrow NO + NO_2 + H_2O + 2Z\text{–}Co \quad [12]$$

$$CO + 1/2O_2 \rightarrow CO_2. \quad [13]$$

(Z = zeolite)

The formation of an adsorbed NO_2 on Co^{2+} sites is a necessary step, which is readily equilibrated with gaseous NO_x under reaction conditions. Our TPD and IR studies suggest CH_4 does not adsorb on a "bare" Co–zeolite at low temperatures. We also found that there was little CH_4 combustion when CH_4 and O_2 were fed over Co–zeolite catalysts at low temperatures. However, the presence of NO or NO_2 enhances the CH_4 conversion in a NO (or NO_2)/CH_4/O_2 feed (39). Further, with Co–ferrierite under differential reaction conditions at 400°C, CH_4 is consumed mainly for NO_x reduction instead of combustion (see Tables 3 and 4) (17). This suggests that NO_x plays a key role in activating CH_4. Perhaps CH_4 is catalytically activated by adsorbed NO_2 species. NO_2 contains an unpaired electron. It is known that NO_2 radicals can remove hydrogen from saturated hydrocarbons, e.g., nitration of CH_4 (forming nitromethane, CH_3NO_2) via a gas-phase NO_2/CH_4 reaction (40). Therefore, it is possible that CH_4 could be activated through a cobalt-bound NO_2 species, e.g.,

NO_2^-, forming $CH_3\cdot$ radicals. The $CH_3\cdot$ radical may be formed by abstraction of a $H\cdot$ from CH_4. This possibly occurs over a nitro species like that described by structure [5A]. The $CH_3\cdot$ radical could react further with a nitrito species (structure [5B]) forming CH_3NO_2. N_2 then forms by reacting the adsorbed CH_3NO_2 with a gas-phase NO molecule (Eq. [10]). Z–Co–HNO_2 formed in Eq. [8] can decompose readily to NO, NO_2, and H_2O or convert to HNO_3 (35, 41). CO formed in Eq. [10] is easily oxidized to CO_2 in an oxidizing atmosphere (Eq. [13]), and Z–Co–OH may react with a NO molecule forming Z–Co–HNO_2 (Eq. [11]). Alternatively, CH_3NO_2 can also be readily isomerized and subsequently decomposed on a catalyst. In this regard, Blower and Smith studied catalytic decomposition of nitromethane on metal exchanged zeolites (Na^+, Cu^{2+}, Ni^{2+}, UO_2^{2+}, Zn^{2+}, Mn^{2+}, La^{3+}, Co^{2+}, Cd^{2+} exchanged Y zeolite) (42). The major decomposition products were ammonium salts, H_2O, N_2, CO, and CO_2.

From the point of view of making a N–N bond, the possibility of formation of N_2O_3 as an intermediate cannot be excluded. N_2O_3 may be formed by coupling of a gas-phase NO with a nitrito group (structure [5B]), then N_2O_3 may react with $CH_3\cdot$ radicals forming N_2, CO_2, and H_2O. However, N_2O_3 is extremely unstable due to its unusually long N–N bond (0.186 nm) (41); it decomposes to NO and NO_2 at $T > -30$°C. In the liquid state, N_2O_3 may also undergo self-ionization formfing NO^+ and NO_2^- (43). If N_2O_3 forms on catalyst under reaction conditions, one might expect its conversion to two ionic species, $NO^{\delta+}$ and $NO_2^{\delta-}$. On the other hand, although covalent N_2O_5 was detected during NO_2 adsorption (Fig. 6), the molecular form of N_2O_5 is not sufficiently stable to contribute to the NO_x catalysis. In fact N_2O_5 readily decomposes to two ionic species (NO_2^- and NO_3^-) upon interaction with a third body (33). Both species have the ability to activate CH_4 forming nitromethane (40). In our work, the presence of NO_2^+ (~2375 cm^{-1} (34)) was not positively identified on Co–ferrierite by IR, whereas NO_3^- was detected.

For our studies with Co–ZSM-5 and Co–ferrierite, the rate-determining step must include the cleavage of the C–H bond (Eq. [8]), especially at low temperatures (350–450°C), whereas the formation of catalyst bound NO_2 (Eq. [5]) can occur quite readily in this temperature range and is thermodynamically favored. The decomposition of a reaction intermediate (C–N species), e.g., CH_3NO_2 can also occur quite readily at moderate conditions and should not be a rate-determining step. At high temperatures (>500°C), the decreased population of NO_2 species on catalyst, due to desorption and conversion to NO, severely limits the overall reaction rate. Therefore, a slower increase in the NO_x conversion curve occurs (17) with increasing temperature. A side reaction, i.e., CH_4 combustion, can proceed with a parallel path on separate Co^{2+} sites. It does not alter the rate-determining step but decreases the effective concentration of CH_4, thus decreasing the NO_x reduction rate. Similarly, water has a significant impact on the NO_x reduction rate but does not affect the rate determining step; water simply reduces the sites available for NO_x reduction.

The above analysis of the rate-determining step is also consistent with the recent work of Cant and co-workers (44). They studied NO reduction using CH_4 and CD_4 in the presence of excess O_2 over a Co–ZSM-5 catalyst and found that the ratio of CH_4 to CD_4 consumption is ~2.4 with a dry feed (1640 ppm NO, 2.5% O_2, 1040 ppm CH_4 or CD_4) at 375°C. This ratio was 2.1 when a wet feed (1.6% H_2O) was used at 431°C. These ratios are close to those expected for a primary kinetic isotope effect. They concluded that the rate-determining step must be the breakage of a C-H bond in the CH_4 molecule. Our work suggests that this C–H bond breakage may be facilitated by surface NO_2 species.

CONCLUSIONS

The valence state of cobalt in Co–zeolite was found to be 2+ and is relatively stable against redox treatment. NO adsorbed on Co–zeolites is dominated by the dinitrosyl species, at ~1810 cm^{-1} (asymmetric stretch) and at 1890–1897 cm^{-1} (symmetric stretch). The dinitrosyls on Co–ferrierite are unusually stable, which may be attributed to the large dinitrosyl angle, ~130°, compared to that of copper–ZSM-5 dinitrosyls, ~104°. The mononitrosyl species on Co–ferrierite at 1930 cm^{-1} is unstable at room temperature. Oxygen can stabilize this cobalt–mononitrosyl, and this may be a result of co-adsorption of oxygen on the Co^{2+} ion. In oxygen both dinitrosyls and mononitrosyl convert to catalyst-bound NO_2 species at elevated temperatures, and this adsorbed NO_2 species is suspected to be crucial in activating CH_4 (breaking a C–H bond). A mechanistic scheme was proposed involving the formation of $CH_3\cdot$ as a key step and a nitro species as an intermediate.

ACKNOWLEDGMENTS

Thanks are due to Dr. Paula Clark for XPS experiments and to Dr. Frank Petrocelli for helpful discussions about IR experiments. We thank Air Products and Chemicals, Inc. for permission to publish this work.

REFERENCES

1. Held, W., Konig, A., Richter T., and Ruppe, L., SAE Paper No. 900496, 1990.
2. Hamada, H., Kintaichi, Y., Sasaki, M., Ito, T., and Tabata, M., *Appl. Catal.* **64,** L1 (1990).
3. Kintaichi, Y., Hamada, H., Tabata, M., Sasaki, M., Ito, T., *Catal. Lett.* **6,** 39 (1990).
4. Hamada, H., Kintaichi, Y., Sasaki, M., Ito, T., and Tabata, M., *Appl. Catal.*, **70,** L15 (1991).

5. Misono, M., and Kondo, K., *Chem. Lett.* 1001 (1991).
6. Sato, S., Yu-u, Y., Yahiro, H., Mizuno, N., and Iwamoto, M., *Appl. Catal.* **70,** L1 (1991).
7. Sato, S., Hirabay, H., Yahiro, H., Mizuno, N., and Iwamoto, M., *Catal. Lett.* **12,** 193 (1992).
8. Bennett, C. J., Bennett, P. S., Golunski, S. E., Hayes, J. W., and Walker, A. P., *Appl. Catal. A* **86,** L1 (1992).
9. Bartholomew, C. H., Gopalakrishnan, R., Stafford, P. R., Davison, J. E., and Hecker, W. C., AIChE 1992 Annual Meeting, Nov. 1-6, 1992, Miami Beach, FL. Paper No. 240a.
10. d'Itri, J. L., and Sachtler, W. M. H., *Catal. Lett.* **15,** 289 (1992).
11. Ansell, A. P., Diwell, A. F., Colunski, S. E., Hayes, J. W., Rajaram, R. R., Truex, T. J., and Walker, A. P., *Appl. Catal. B* **2,** 81 (1993).
12. Burch, R., and Millington, P. J., *Appl. Catal. B* **2,** 101 (1993).
13. Li, Y., and Armor, J. N., *Appl. Catal. B* **1,** L31 (1992).
14. Li, Y., and Armor, J. N., *Appl. Catal. B* **2,** 239 (1993).
15. Li, Y., and Armor, J. N., *Appl. Catal. B* **3,** L1 (1993).
16. Petunchi, J., Sill, G., and Hall, W. K., *Appl. Catal. B* **2,** 303 (1993).
17. Li, Y., and Armor, J. N., *J. Catal.* **150,** 376 (1994).
18. Armor, J. N., and Li, L., *in* "Proc. Sym. on NO_x Reduction," ACS Meeting, San Diego, CA, Mar. 13–18, 1994.
19. Iwamoto, M., *in* "Future Opportunities in Catalytic and Separation Technologies" (M. Misono, Y. Moro-oka and S. Kimura Eds.), p. 121. Elsevier, Amsterdam, 1990.
20. Li, Y., and Hall, W. K., *J. Catal.* **129,** 202 (1991).
21. Armor, J. N., and Li, Y. *in* "Proc. Sym. NO_x Reduction," ACS Meeting, San Diego, Mar. 13–18, 1994.
22. Iwamoto, M., Yahiro, H., Mizumo, N., Zhang, W.-X., Mine, Y., Furukawa, H., and Kagawa, S., *J. Phys. Chem.* **96,** 9360 (1992).
23. Valyon, J., and Hall, W. K., *in* "Proceedings, 10th International Congress Catalysis Budapest, 1992 (L. Guczi, F. Solymosi, and P. Tétényi, Eds.). Akadémiai; Kladó, Budapest, 1993.
24. Valyon, J., and Hall, W. K., *J. Phys. Chem.* **97,** 1204 (1993).
25. Valyon, J., and Hall, W. K., *Catal. Lett.* **15,** 311 (1992).
26. Spoto, G., Bordiga, S., Scarano, D., and Zecchina, A., *Catal. Lett.* **13,** 39 (1992).
27. Giamello, E., Murphy, D., Magnacca, G., Morterra, C., Shioya, Y., Nomura, T., and Anpo, M., *J. Catal.* **136,** 510 (1992).
28. Windhorst, K. A., and Lunsford, J. H., *J. Am. Chem. Soc.* **96,** 1407 (1975).
29. Lunsford, J. H., Hutta, P. J., Lin, M. J., and Windhorst, K. A., *Inorg. Chem.* **17,** 606 (1978).
30. Praliaud, H., Coudurier, G. F., and Taarit, Y. B., *J. Chem. Soc., Faraday Trans. 1* **74,** 3000 (1978).
31. Xu, Q., Millman, W. S., and Hall, W.K., unpublished work.
32. Fierro, J. L. G., *in* Spectroscopic Characterization of Heterogeneous Catalysis" (J. L.G. Fierro, Ed.), p. B166. Elsevier, Amsterdam, 1990.
33. Horn, A. B., Kock, T., Chester, M. A., McCoustra, M. R. S., and Sodeau, J. R., *J. Phys. Chem.* **98,** 946 (1994).
34. Nakamoto, K., "Infrared Spectra of Inorganic and Coordination Compounds," Wiley–Interscience, New York, 1970.
35. Cotton, F. A., and Wilkinson, G., "Advanced Inorganic Chemistry," 4th ed. Wiley–Intersciences, New York, 1980.
36. MaIntyre, N. S., and Cook, M. G., *Anal. Chem.* **47,** 2208 (1975).
37. Tøpsøe, N.-Y., and Tøpsøe, H., *J. Catal.* **75,** 354 (1982).
38. Armor, J. N. and Li, Y., Presentation at Pittsburgh–Cleveland Catal. Soc. Meeting, May 1994, Pittsburgh, PA.
39. Li, Y., and Armor, J. N., unpublished work.
40. Olah, G. A., Malhotra, R., and Suhash, C. N., "Nitration Methods and Mechanisms, VCH, New York, 1989.
41. Wells, A. F., "Structural Inorganic Chemistry," 5th ed., p. 816. Clarendon Press, Oxford, 1984.
42. Blower C. J., and Smith, T. D., *Zeolites* **13,** 396 (1993).
43. Shaw, A. W., Vosper, A. J., and Pritchard, M., *J. Chem. Soc., Dalton, Trans.* 2172 (1974).
44. Cowan, A. D., Dumpelmann, R., and Cant, N. W., private communication.